Influence of oxygen partial pressure and annealing temperature on the physical properties of nanostructured ZnO thin films prepared by RF magnetron sputtering

R. Subba Reddy[1], S. Uthanna[1], A. Sivasankar Reddy[2], T. Srikanth[2], B. Radha Krishna[3]

[1]*Department of Physics, Sri Venkateswara University, Tirupati 517 502, India*
[2]*Department of Physics, Vikrama Simhapuri University PG Center, Kavli 524 201, India*
[3]*Department of Physics, NBKR Institute of Science and Technology, Vidyanagar 524413, India*

*Corresponding author

DOI**:** 10.5185/amp.2018/1416
www.vbripress.com/amp

Abstract

Zinc oxide thin films were deposited by RF magnetron sputtering on p-type (100) silicon and glass substrates held at room temperature by varying the oxygen partial pressures and the optimized films was annealing at different temperatures. The deposition rate of the films was decreased from 5.8 to 2.5 nm /min with increase of oxygen partial pressures. X- ray diffraction results reveal that the films deposited at oxygen partial pressure of $2x10^{-2}$ Pa the (100) preferred orientation peak crystallinity became better. Raman spectroscopy analysis shows an improvement in the crystalline quality of the films at $2x10^{-2}$ Pa. Fourier transform infrared spectroscopy of ZnO films confirms the presence Zn-O bonding. The nanorods were observed at oxygen partial pressure of $5x10^{-2}$ Pa. The maximum transmittance of 97% and crystallite size of 21 nm was observed at oxygen partial pressure of $2x10^{-2}$ Pa. The as deposited films annealed at 473 K the intensity of (100) phase was decreased. The RMS roughness of the as deposited ZnO films was 7.3 nm, and it increased to 30 nm for the films annealed at 473K. Optical spectra revealed the films annealed at 673 K show the optical band gap of 3.17 eV.

Keywords: Zinc oxide, nanocrystalline, nanorods, thin films, structure.

Introduction

Zinc oxide (ZnO) is a direct transition compound semiconductor having a hexagonal wurtizite structure, a wide energy band gap, abundance in nature, lack toxicity, environment friendliness, excellent piezoelectric and optical properties [**1**]. Recently, nanostructured zinc oxide thin films have been investigated due to their potential applications such as solar cells and transparent electrodes [**2**], photo detectors, LEDs, field effect transistors (FETs) sensors [**3**], and surface acoustic wave devices [**4-6**]. Thin films of ZnO were prepared using various deposition techniques such as electron beam evaporation, molecular beam epitaxy, atomic layer deposition technique, pulsed laser deposition, spray pyrolysis, metal organic chemical vapour deposition, DC and RF magnetron sputtering [**7-14**] etc. Among these methods, RF magnetron sputtering is a best method to prepare transparent conducting oxide (TCO) thin films due to the reason of good adhesion to the substrate, good uniformity thickness control and better reproducibility of films. The properties of the sputtered films are strongly influenced by process parameters such as sputtering power, oxygen partial pressure, substrate temperature, etc. In this investigation, nanocrystalline ZnO thin films were prepared by RF magnetron sputtering and study the oxygen partial pressure and annealed temperature influenced structural and morphological and optical properties.

Experimental

ZnO thin films were deposited on silicon (100) and glass substrates by using RF magnetron sputtering system. Pure metallic zinc target 2 inch (5 cm) was used for deposition of the ZnO films. The magnetron sputtering system is capable of producing base pressure of $2x10^{-4}$ Pa using diffusion pump and rotary pump combination and a liquid nitrogen trap. All samples were deposited at room temperature (303 K). The pressure in the chamber was measured with digital Pirani gauge and Penning gauge. The target to substrate distance was kept at 50 mm for all the depositions. High purity (99.99%) argon and oxygen were used as sputter and reactive gasses respectively. ZnO thin films

were deposited on silicon and Corning glass substrates at different oxygen partial pressures in the $5x10^{-3}$Pa – $5x10^{-2}$Pa range. The silicon and glass substrates (26mmx18mmx1mm) were rinsed in acetone and in acid solution (1/3 HCl**:** 2/3HNO_3) then were ultrasonically cleaned. Before deposition of films, the zinc target was presputtered in argon atmosphere for about 10 min in order to remove the surface oxide layer of the target. The optimized films were annealed in air for 1 hour at 473 and 673 K. The process parameters maintained during growth of the films are given below **Table 1**.

Table 1. Deposition parameters for the growth of ZnO films.

Sputter target	:	Zn
Target to substrate distance	:	50mm
Base pressure	:	$2x10^{-4}$ Pa
Oxygen partial pressure (pO_2)	:	$5x10^{-3}$ Pa- $5x10^{-2}$ Pa
Annealed temperatures	:	473 and 673 K
Sputter pressure	:	5 Pa
Substrate temperature	:	303 K
Sputter power	:	150 W
Deposition time	:	60 min

The deposited thin films thickness was measured by using of α- step profilometer, the crystallographic structure of the films was determined with glancing angle X- ray diffraction (XRD) taken on a Brurker D8 Advance Diffractometer at the glancing angle of 4^0 using monochromatic Co $K\alpha_1$ radiation (λ = 1.78897 Aº). The surface morphology of the films was analyzed by atomic force microscopy (AFM) and scanning electron microscopy (SEM). Fourier transform infrared spectroscopic (FTIR) measurements in the wave number range between 400 and 4000 cm^{-1} were carried out using Nicolet Magana IR 750, FTIR spectrometer. Raman spectra were measured in back scattering configuration with an Ar^+ ion laser of 514.5 nm (Renishaw, RM 2000) which were used to examine the change of crystallinity. The optical transmittance of the films was recorded using US-Vis-NIR Perkin – Elmer double beam spectrophotometer in the wavelength range 300 - 2500 nm.

Results and discussion

Effect of oxygen partial pressure

The deposition rate of the ZnO films decreased from 5.8 nm/ min to 2.5 nm/ min with increase of oxygen partial pressure from $5x10^{-3}$ to $5x10^{-2}$ Pa. With increase of oxygen partial pressure the decrease of deposition rate was due to reason of oxidation of target led to low sputter yield. The oxidation reaction between the oxygen molecules and ejected atoms from Zn target would be enhanced, consequently the deposition rate was decreased with increase of oxygen content. The highest deposition rate 5.8 nm/ min was obtained at low oxygen concentration was due to enhance the bombardment of the positive ions to a films. The bombardments of the positive argon ions with appropriate kinetic energies assisted the crystallization process of ZnO films, resulting in an increase in the deposition rate of the ZnO films [**15**].

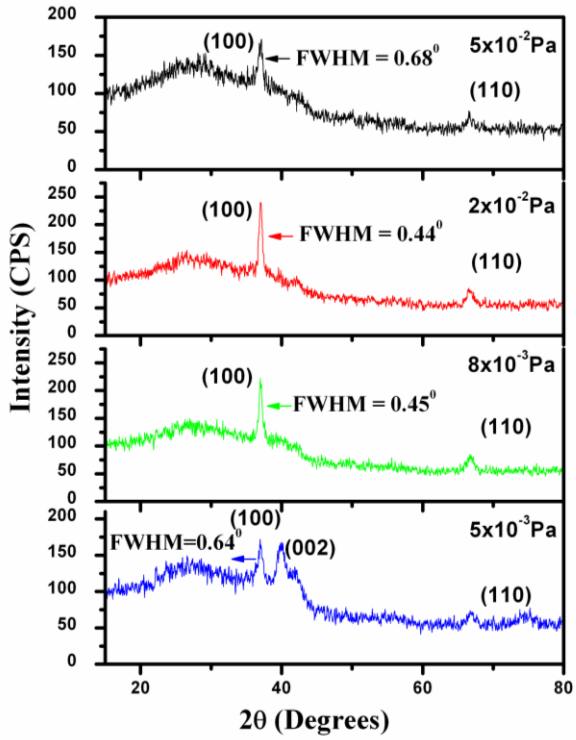

Fig. 1. XRD patterns of ZnO films deposited at various oxygen partial pressures.

Structural properties

Fig.1. shows the X-ray diffraction profiles of ZnO thin films deposited at different oxygen partial pressures in the range of $5x10^{-3}$ - $5x10^{-2}$ Pa. The films formed at oxygen partial pressure of $5x10^{-3}$ Pa consists of the weak reflections (100), (002) and (110) indicated the growth of nanocrystalline with hexagonal structure of ZnO films. With increase of oxygen partial pressure to $2x10^{-2}$ Pa the intensity of (100) reflection increased and the (002) reflection disappeared. Beyond this oxygen partial pressure the intensity of (100) reflection decreased, which was due to the inhibition of the grain growth by excess oxygen segregation at the grain boundaries [**16**]. The films deposition at oxygen partial pressure of $2x10^{-2}$ Pa the (100) peak becomes sharper due to improvement in stoichiometry of the film, associated with the incorporation of oxygen at oxygen vacancies [**17**].

The full width at half maximum (FWHM) value of the (100) peak decreased from 0.64^0 to 0.44^0 and then increased to 0.68^0 with the increasing of oxygen partial pressure. The crystallite size of the films increased from 15 to 22 nm and then decreased to 14 nm with the increase of oxygen partial pressure from $5x10^{-3}$ to $5x10^{-2}$ Pa. The maximum crystallite size was achieved at oxygen partial pressure of $2x10^{-2}$ Pa due to its smallest FWHM. Crystallite size of the films has been calculated using the Scherror's equation [**18**].

$$L = 0.9\,\lambda/\,ß\cos\theta \quad (1)$$

where λ is the wavelength of the X- rays (Co $K\alpha_1$ radiation, λ = 1.78897 A°), ß the full width at half maximum of the peak and θ the Bragg diffraction angle. Dislocation density and strain calculated by using below equations [19.

$$\text{Dislocation density } (\delta) = 1/L^2 \quad (2)$$

$$\text{Strain } (\varepsilon) = \beta\cos\theta/4 \quad (3)$$

here ß is the full width half maximum of the peak and θ is the Bragg diffraction angle and L is crystallite size.

The dislocation density of ZnO films first decreased from 44 to 21 lines/ m^2 and then increased to 53 x 10^{-4} lines/ m^2 with increase of oxygen partial pressure. The strain also first decreased from 26 to 17x10^{-4} $line^{-2}$ m^{-4} and then increased to 28 x 10^{-4} $line^{-2}$ m^{-4} with increase of oxygen partial pressure from 5x10^{-3} to 5x10^{-2}Pa. The strain decreased at oxygen partial pressure of 2x10^{-2} Pa was due to the increases of the film crystallinity [**19**]. The obtained crystallite size, FWHM, strain and dislocation density are listed in **Table 2**.

Table 2. Crystallite size, FWHM, strain, dislocation density and band gap values of ZnO films at different oxygen partial pressures.

pO_2 (mbar)	crystallite size (nm)	FWHM (degree)	Strain (ε) ($line^{-2}$ m^{-4})	Dislocation density (δ) (lines/ m^2)	Band gap Eg (eV)
5x10^{-3}	15	0.64	26	44	3.04
8x10^{-3}	20	0.47	19.4	25	3.07
2x10^{-2}	22	0.44	17.2	21	3.10
5x10^{-2}	14	0.68	28	53	3.14

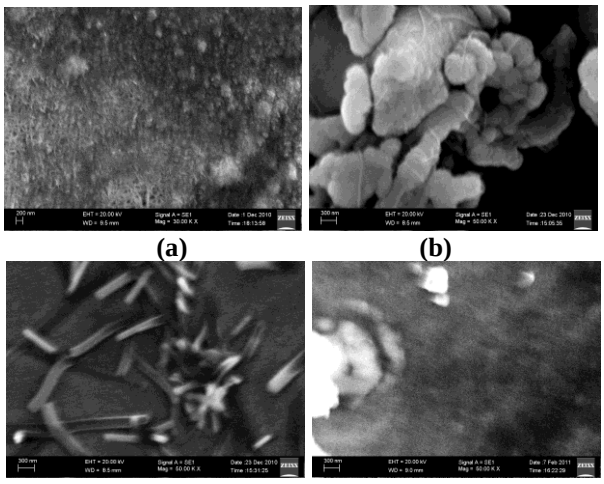

Fig. 2. SEM images of ZnO films (a) 5x10^{-3} Pa (b) 8x10^{-3} Pa (c) 2x10^{-2} Pa (d) 5x10^{-2} Pa.

SEM analysis

Fig. 2 shows SEM images of ZnO thin films at different oxygen partial pressures. The nanorods were formed at oxygen partial pressure of 5x10^{-2} Pa. These rods are about 1.2 µm and 150 nm thick. Li *et al.* [15. reported the nanorods were formed at Ar/O mixture of 10/30, the nanorods average length about 1µm and 50 nm thick. The oxygen partial pressure decreased to 2x10^{-2} Pa the nanorods were disappeared and formed small grain with dense surface. Further decrease of oxygen partial pressure to 8x10^{-3} Pa nanoflowers type structures were formed. At low oxygen partial pressure of 5x10^{-3} Pa the films exhibited porous morphology with spherical particles of average size about 80 nm formed perpendicular to the films surface due to appearance c-axis (002) orientation of ZnO. **Fig. 3** shows EDS spectra at different oxygen pressures. The atomic percent of Zn was decreased with increase of oxygen pressure from 5x10^{-3} Pa to 5x10^{-2} Pa due to increase of oxygen content.

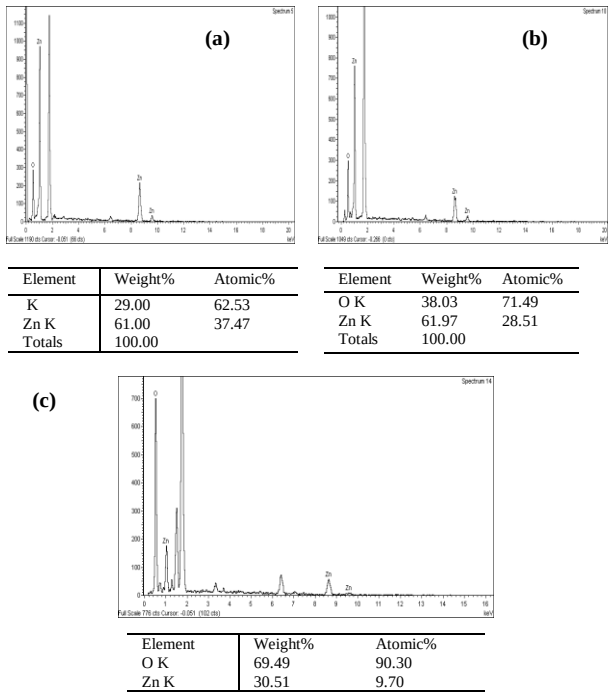

Element	Weight%	Atomic%
K	29.00	62.53
Zn K	61.00	37.47
Totals	100.00	

Element	Weight%	Atomic%
O K	38.03	71.49
Zn K	61.97	28.51
Totals	100.00	

Element	Weight%	Atomic%
O K	69.49	90.30
Zn K	30.51	9.70

Fig. 3. EDS spectra of ZnO films (a) 5x10^{-3} Pa (b) 2x10^{-2} Pa (c) 5x10^{-2} Pa.

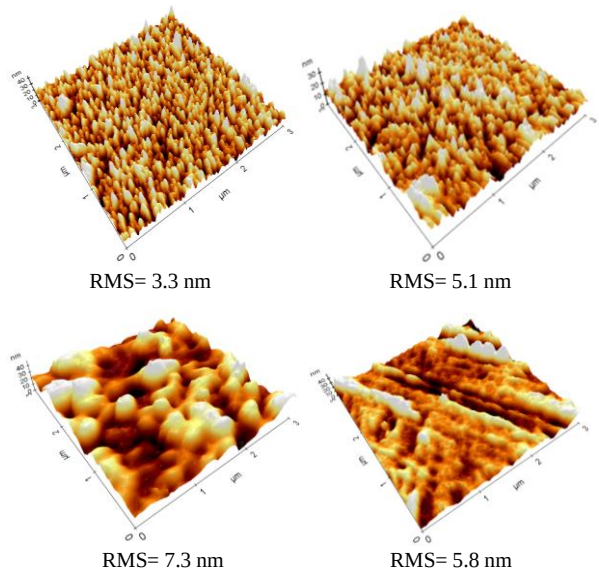

Fig. 4. AFM images of ZnO films (a) 5x10^{-3} Pa (b) 8x10^{-3} Pa (c) 2x10^{-2} Pa (d) 5x10^{-2} Pa.

AFM analysis

AFM images of ZnO films deposited at different oxygen partial pressures are shown in **Fig. 4**. The surface morphology was strongly depending on the oxygen partial pressure. The films deposited at oxygen partial pressure of $5x10^{-3}$ Pa showed lowest root means square (RMS) surface roughness of 3.3 nm. The RMS surface roughness was increased from 3.3 to 7.4 nm with increasing of oxygen partial pressure from $5x10^{-3}$ to $2x10^{-2}$ Pa. The surface morphology of the films confirms a noticeable transformation with increase of oxygen partial pressure.

FTIR analysis

Fig. 5 shows FTIR spectra of ZnO thin films at different oxygen partial pressures. The peak at 410.41 cm^{-1} corresponds to the Zn-O stretching vibration for a hexagonal ZnO formed at oxygen partial pressure of $5x10^{-2}$ Pa. The FTIR spectra of the ZnO films show a strong peak at 408 cm-1. Nandi et al. reported [**21**] the absorption band at 409 cm^{-1} corresponds to Zn-O stretching vibration for a tetrahedral surrounding of Zn atoms. The absorption band shifted to lower wavenumber side with increase of oxygen partial pressure to $5x10^{-2}$ Pa. The optical modes of the Zn-O bonds were decided by the bond length, bond angle, bond strength and atomic coordination numbers. The films deposited at oxygen partial pressure of $8x10^{-3}$ Pa the full width at half maximum (FWHM) was 4.3 cm. With increase of oxygen partial pressure the FWHM was decreased to 3.4 cm and there after increased to 4.6 cm with increase of pO_2 from $2x10^{-2}$ to $5x10^{-2}$ Pa. The larger FWHM value indicates wider distribution of vibration energy of the Zn-O bonds. Similar changes were observed by Wang *et al.* [**22**] in magnetron sputtered ZnO films.

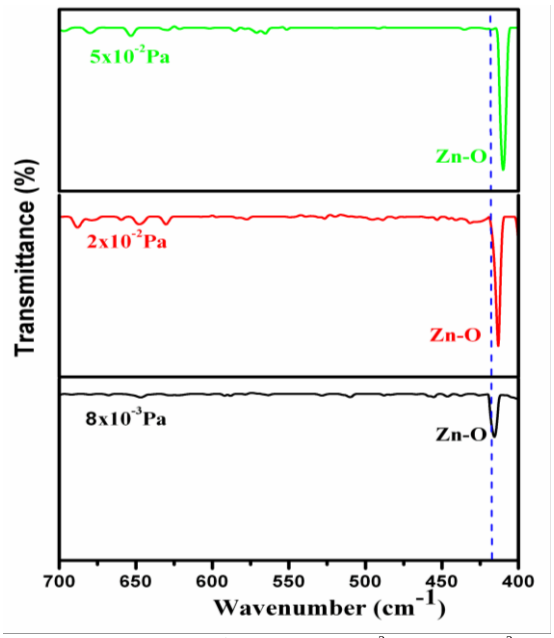

Fig. 5. FTIR spectra ZnO films at (a) $5x10^{-2}$ Pa (b) $2x10^{-2}$ Pa (b) $8x10^{-3}$ Pa.

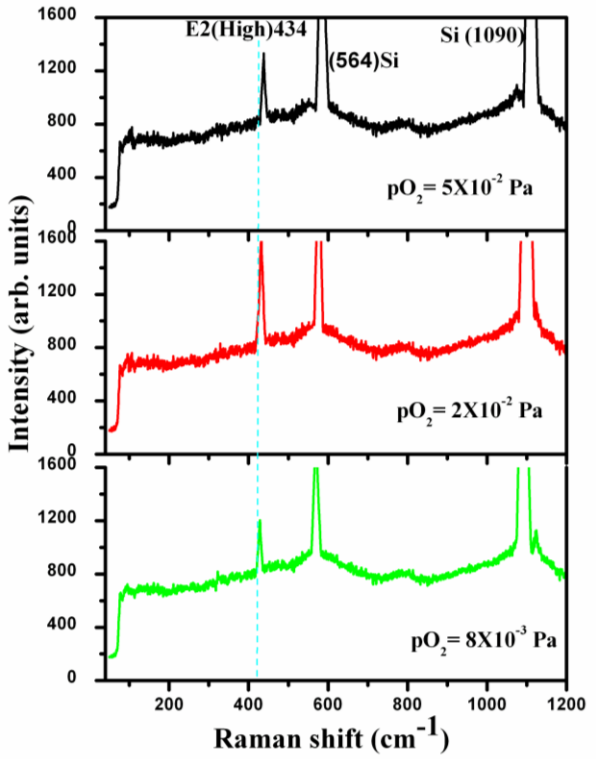

Fig. 6. Raman spectra of ZnO films at different oxygen partial pressures.

Raman analysis

Fig. 6 shows Raman spectra of ZnO thin films deposited on to silicon substrates at different oxygen partial pressures. The peaks at 564 and 1090 cm^{-1} are silicon substrates peaks. The sharp peak at 434 cm^{-1} is a typical characteristic of wurtzite ZnO and assigned to be the Raman active optical- phonon E_2 mode [**23, 24**]. The intensity of the E_2^H peak first increased with increase of oxygen partial pressure to $2x10^{-2}$ Pa and then decreases slightly at higher oxygen partial pressure of $5x10^{-2}$. These results indicated that the films formed at $2x10^{-2}$ Pa exhibits the structural quality, which is good agreement in XRD results. Lei *et al.* [**10**] reported the E_2^H peak 437 cm^{-1} increases with increasing of oxygen partial pressure to 160 m Torr and then decreases slightly.

Optical properties

Fig. 7 shows the optical transmittance spectra of nanostructured ZnO thin films formed at different oxygen partial pressures. The average optical transmittance of ZnO films are nearly 85% and maximum transmittance was 97%. The optical transmittance of ZnO films increased with increase of oxygen partial pressure from $5x10^{-3}$ Pa to $2x10^{-2}$ Pa and then decreased on further increase of oxygen partial pressure to $5x10^{-2}$ Pa. The improvement of optical transmittance with oxygen partial pressure indicates the films stoiciometry is gradually improved as increase of oxygen ratio in the total pressure ($Ar+O_2$). The lower transmittance of the film grown under oxygen deficient

condition originates from the defeat electronic states with in the band gap associated with oxygen vacancies and interstitial Zn atoms [**16**]. The sharp absorption band edge was observed around 423 nm in the films formed at oxygen partial pressure of $5x10^{-3}$ Pa. The absorption band edge was shifted to lower wavelength side with the increase of oxygen partial pressure from $5x10^{-3}$ Pa to $5x10^{-2}$ Pa. The optical band gap (Eg) can be calculated from equ (5).

$$\text{The absorption co efficient } (\alpha) = \ln (T/d) \quad (4)$$

where d is the film thickness, the optical band gap can be calculated from the following expression [20.

$$\alpha h\nu = A(h\nu - Eg)^m \quad (5)$$

where m = ½ for the direct band gap

The optical band gap (Eg) of ZnO thin films increased from 3.04 to 3.14 eV with the increase of oxygen partial pressure from $5x10^{-3}$ to $5x10^{-2}$ Pa (**Table 2**). Wang *et al.* [**22**] observed the band gap increased with increase of oxygen partial pressure from 0 sccm to 10 sccm was due to the decrease of defects. The presence of vacancies and dopants decreases the band gap of the ZnO films.

The refractive index (n) of the films was measured from the optical transmittance interference data employing Swanepoel's envelope method [**25**] using the relation

$$n(\lambda) = [N + (N^2 - n_0^2 n_1^2)^{1/2}.^{1/2} \quad (6)$$

and

$$N = 2n_0 n_1 [(T_M - T_m)/T_M T_m. + (n_0^2 + n_1^2)^{1/2} \quad (7)$$

where T_M and T_m are the optical transmittance maximum minimum respectively. In general, refractive index of the films was increased with the increase of photon energy. The refractive index was decreased from 1.86 to 1.83 with increase of wavelength 500 to 700 nm and remains almost constant.

From the above results, the films deposited at the oxygen partial pressure of $2x10^{-2}$ Pa exhibited better properties then other conditions, hence these films are annealed at 473K and 673K.

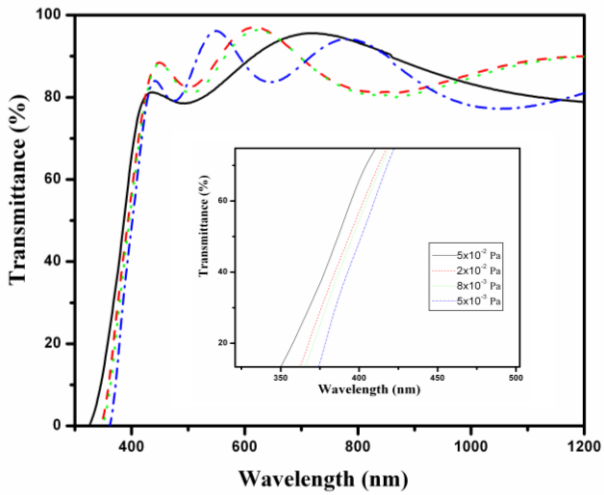

Fig.7. Optical transmittance spectra of ZnO films at different oxygen partial pressures.

Effect of annealing temperatures

Structural analysis

Fig. 8 shows the X-Ray diffraction (XRD) patterns of as deposited and annealed ZnO films. From the XRD patterns, films deposited at room temperature consists (100), (110) orientation of ZnO. The as deposited films annealed at 473K the intensity of (100) phase decreased. Senadim *et al.* [**26**] reported that the (100) peak intensity decreased with increase in the annealing temperature due to the heating of the surface leads to desorption of oxygen. Further increase of annealing temperature to 673 K the intensity of (100) peak enhanced due to the heat treatment process improved the crystallinity of existing grains [**27**]. The FWHM increased from 0.44 to 1.0^0 and then decreased to 0.58^0 with increase of annealing temperature from 303 to 673 K.

The obtained crystallite size values are 21, 9.6 and 16 nm for the annealing temperature of 303, 473 and 673 K, respectively. The improvement of crystallite size may be due to the grain growth and improvement of crystallinity. The annealing process clearly produces a recovery of the crystal structure and increase of the grain size [**28**].

The dislocation density of ZnO films increased from 22.7 to 108 × 10^{-4} lines/ m^2 and then decreased to 40.1 × 10^{-4} lines/m^2 with increase of annealing temperature from 303 to 673 K. The strain also increased from 18.1 to 41.2 × 10^{-4} $line^{-2}$ m^{-4} and then decreased to 23.9 × 10^{-4} $line^{-2}$ m^{-4} with increases of annealing temperature from 303 to 673 K.

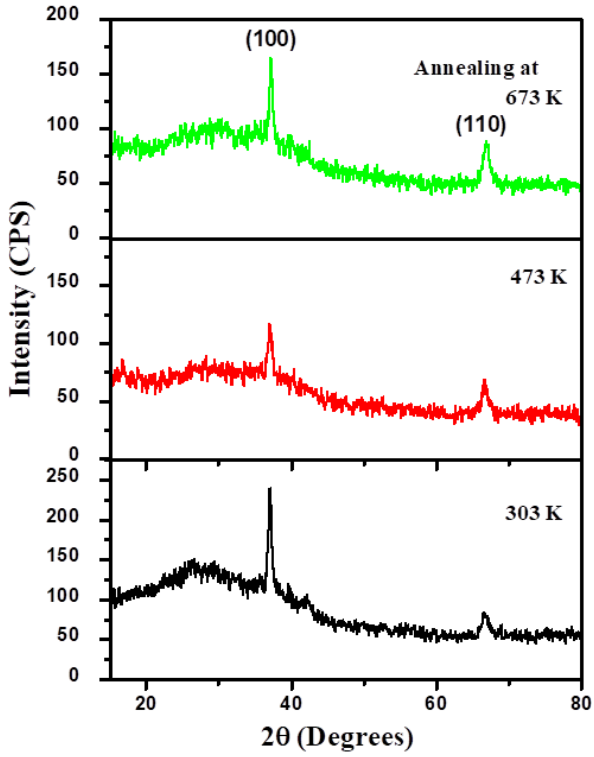

Fig. 8. XRD patterns of ZnO films deposited at various annealing temperatures.

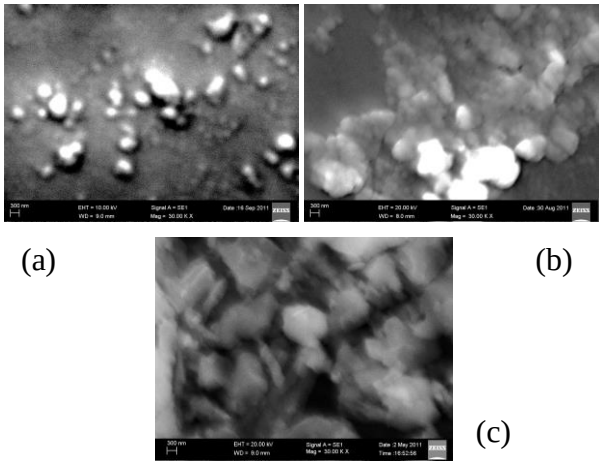

Fig. 9. SEM images of ZnO films (a) 303 (b) annealed at 473 C (c) annealed at 673 K.

SEM analysis

Fig. 9 shows the scanning electron microscopy (SEM) images of as deposited and annealed films. The as deposited films show porous like structure with small nanograins. The films annealed at 473 K shows the circular size of nanocrystals and its size was increased with increasing of annealing temperature to 673 K due to improvement of crystallinity. The formation of nanocrystals in SEM image due to reason the films appear smoother and re- crystallization occurred on the films surface [**29**].

AFM analysis

The root mean square (RMS) roughness was from the atomic force microscope (AFM) measurements for 303, 473 and 673 K. The RMS roughness of as deposited ZnO films was 7.3 nm, and it increased to 30 nm for the films annealed at 473 K. Further increase of annealing temperature to 673 K the RMS roughness decreased to 8.5 nm. The reduction of RMS roughness with annealing temperature is attributed to island coalescence [**30**]. The annealing process clearly produced a recovery of the crystal structure and increase of the grain growth.

FTIR analysis

Fig. 10 shows the FTIR spectra of ZnO films at different annealing temperatures. The as deposited films exhibited a peak at 413 cm^{-1} corresponds to the Zn-O stretching vibration for a tetrahedral surrounding of Zn atoms. On increasing of annealing temperature to 473 K the absorption peak FWHM increased from 7.6 to 10.9 cm^{-1}. Further increases of annealing temperature from 473 to 673 K the FWHM of the absorption peak decreased to 9.1 cm^{-1} due to improvement of better crystallinity. Sha *et al.* [**31**] reported that the absorption peak becomes sharper and its full width at half-maximum decreases with increasing of annealing temperature was due to improvement of the stoichiometric of the films.

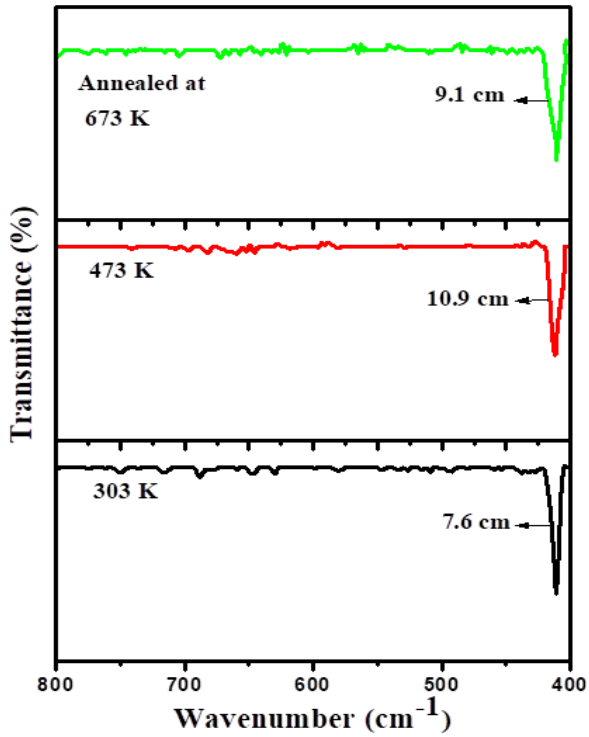

Fig. 10. FTIR spectra of ZnO films at different annealing temperatures.

Optical properties

The as deposited and annealed films shows average optical transmittance of 85 % in the visible region. It was observed from the optical transmittance spectra, the transmission edge is not significantly affected by the annealing temperatures at shorter wavelength. The optical band gap lies between 3.18 eV to 3.16 eV for the as deposited and annealed films. The change of optical band gap with increasing annealing temperature was also observed by Daniel *et al.* [**32**] in rf magnetron sputtered ZnO films.

Conclusions

Highly transparent ZnO thin films have been successfully deposited on the silicon and glass substrates by using RF magnetron sputtering at different oxygen partial pressures and annealing temperatures. AFM and XRD characterization of the films revealed largest RMS roughness, better crystallinity obtain at oxygen partial pressure of $2x10^{-2}$ Pa. With increasing of oxygen partial pressure the (002) orientation disappeared indicates the ZnO nanorods grown parallel to the substrate. The optical band gap of ZnO films increased from 3.04 to 3.14 eV with increase of oxygen partial pressure. SEM analysis reveals circular size of nanocrystals were formed at post deposit annealing of 673 K. FTIR spectra shows the absorption peak at 413 cm^{-1} corresponds to the Zn-O stretching for a tetrahedral surrounding of Zn atoms. The optical band gap of ZnO films was slightly varied with increasing of annealing temperatures.

References

1. Kang, S.J.; Joung, Y.H.; *Appl. Surf. Sci*., **2007**, *253*, 7330. **DOI:** 10.1016/j.apsusc.2007.03.020
2. Matsuda, T.; Furuta, M.; Hiramatsu, T.; Furuta, H.; Li, C.; Hirao, T.; *Appl. Surf. Sci*., **2010**, *256*, 6350.
3. Manjunatha, S.; Panchakarla, L.S.; K. Biswas Rao, C.N.R.; *Inorganica Chimica Acta*, **2010**, *363*, 2696. **DOI:** 10.1016/j.ica.2010.09.008
4. Jeong, S.H.; Yoo, D.G.; Kim, D.Y.; Lee, N.E.; Boo, J.H.; *Thin Solid Films*, **2008**, *516*, 6598. **DOI:** 10.1016/j.tsf.2007.11.034
5. Ma, X.; Zhang, J.; Lu, J.; Ye, Z.; *Appl. Surf. Sci*., **2010**, *257*, 1310. **DOI:** 10.1016/j.apsusc.2010.08.057
6. Liu, H.; Avrutin, V.; Izyumskaya, N.; Ozgur, O.; Morkoc, H.; *Superlatt. Microstruct.*, **2010**, *48*, 458. **DOI:** 10.1016/j.spmi.2010.08.011
7. Kumar, R.R.; Narasimha Rao, Y.; Rajanna, K.; Phani, A.R.; *Mater. Res. Bull.*, **2014**, *52*, 167. **DOI:** 10.1016/j.materresbull.2014.01.022
8. Chen, M.; Zhu, A;. Chen, Z.; Shen, Z.; *Mater. Res. Bull.*, **2016**, *78*, 16. **DOI:** 10.1016/j.materresbull.2016.02.012
9. Jian, S.R.; Lee, Y.H.; *J. Alloys compd.*, **2014**, *587*, 313. **DOI:** 10.1016/j.jallcom.2013.10.213
10. Kumarakuru, H.; Cherns, D.; Collins, A.M.; *Ceramic Internationals*, **2014**, *40*, 8389. **DOI:** 10.1016/j.ceramint.2014.01.045
11. Anandi, R.; Mohan, R.; Swaminathan, K.; Ravichandran, K.; *Superlatt. Microstruct.*, **2012**, *51*, 680. **DOI:** 10.1016/j.spmi.2012.02.006
12. Lee, C.H.; Choi, M.S.; *Thin Solid Films*, **2016**, *605*, 157. **DOI:** 10.1016/j.tsf.2015.09.050
13. Gonçalves, R.S.; Barrozo, P.; Cunha, F.; *Thin Solid Films*, **2016**, *616*, 265. **DOI:** 10.1016/j.tsf.2016.08.040
14. Manouchehri, I.; Mehrparvar, D.; Moradian, R.; Gholami, K.; Osati, T.; *Optik- International Journal for Light and Electron Optics*, **2016**, *127*, 8124. **DOI:** 10.1016/j.ijleo.2016.06.005
15. Li, C.; Matsuda, T.; Kawaharamura, T.; Furuta, H.; Furuta, M.; Hiramatsu, T.; Hirao, T.; *J. Vac. Sci. Technol. B*, **2010**, *28*, 135. **DOI:** 10.1116/1.3259843
16. Hong, R.; Qi, H.; Huang, J.; He, H.; Fan Z.; Shao, J.; *Thin Solid Films*, **2005**, *473*, 58. **DOI:** 10.1016/j.tsf.2004.06.159
17. Teng, X.; Fan, H.; Pan, S.; Ye, C.; Li, G.; *Mater. Lett.*, **2007**, *61*, 201. **DOI:** 10.1016/j.matlet.2006.04.031
18. Cullity, B.D.; Elements of X-ray Diffraction, second ed., Addison Wesley, London, **1978**. **DOI:** 10.1107/S0567739479000917
19. Lalita, S.; Sathyamurthy, R.; Senthilarasu, S.; Subbarayan, A.; Natarajan, K.; *Solar Energy Material & Solar Cells*, **2004**, *82*, 187. **DOI:** 10.1016/j.solmat.2004.01.017
20. Yu, C.F.; sung, C.W.; Chen, S.H.; Sun, S.J.; *Appl. Surf. Sci.*, **2009**, *256*, 792. **DOI:** 10.1016/j.apsusc.2009.08.061
21. Nandi, S.K; Chakraborty, S.; Bera, M.K.; Maiti, C.K.; *Bull. Matter. Sci.*, **2007**, *30*, 247. **DOI:** 10.1007/s12034-007-0044-3
22. Wang, X.C.; Chen X.M.; Yang, B.H.; *J. Alloys compd.*, **2009**, *488*, 232. **DOI:** 10.1016/j.jallcom.2009.08.089
23. Wang, C.Z.; Chen, Z.; Hu, H.; Zhang, D.; *Physica B*, **2009**, *404*, 4075. **DOI:** 10.1016/j.physb.2009.07.165
24. Yin, Z.; Chen, N.; Dai, R.; Liu, L.; Zhang, X.; Wang, X.; Wu, J.; Chai, C.; *J. Cryst. Growth*, **2007**, *305*, 296. **DOI:** 10.1016/j.jcrysgro.2007.04.043
25. Swanepoel, R.; *J. Phys. E: Sci. Instrum.*, **1983**, *16*, 1214. **DOI:** 0022-3735/16/12/023
26. Senadim, E.; Kavak, H.; Esen, R.; *J. Phys. Condensed Matter.*, **2006**, *18*, 6391. **DOI:** 10.1088/j.jcrysgro.2007.04.043
27. Pung, S.Y.; Choy, K.L.; Hou, X.; Shan, C.; *Nanotechnol.*, **2008**, *19*, 435609. **DOI:** 10.1088/0957-4484/19/43/435609
28. Roy, C.; Byrne, S.; Mc Glynn, E.; Mosnier, J.P.; Posada, E.d.; Mahony, D.O.; Cafolla, A.A.; *Thin Solid Films*, **2003**, *436*, 273. **DOI:** 10.1016/S0040-6090(03)00617-5
29. Laurent, K.; Yu, D.P.; Nenez, S.T.; Wang, Y.L.; *J. Phys. D: Appl. Phys.*, **2008**, *41*, 195410. **DOI:** 10.1088/0953-8984/18/27/021
30. Bang, K.H.; Hwang, D.K.; Hyang, J.M.; *Appl. Surf. Sci.*, **2003**, *207*, 359. **DOI:** 10.1016/S0169-4332(03)00005-9
31. Sha, Z.D.; Wu, X.M.; Zhuge, L.J.; *Phys. Lett. A*, **2006**, *355*, 228. **DOI:** 10.1016/j.physleta.2006.01.105
32. Daniel, G.P.; Justinvictor, V.B.; Nair, P.B.; Joy, K.; Koshy, P.; Thomas, P.V.; *Physica B*, **2010**, *405*, 1782. **DOI:** 10.1016/j.physb.2010.01.039

